

# Universal spectral behavior of $x^2(ix)^\varepsilon$ potentials

Carl M. Bender\* and Daniel W. Hook†

Department of Physics, Washington University, St. Louis, MO 63130, USA

(Dated: October 31, 2018)

The  $\mathcal{PT}$ -symmetric Hamiltonian  $H = p^2 + x^2(ix)^\varepsilon$  ( $\varepsilon$  real) exhibits a phase transition at  $\varepsilon = 0$ . When  $\varepsilon \geq 0$ , the eigenvalues are all real, positive, discrete, and grow as  $\varepsilon$  increases. However, when  $\varepsilon < 0$  there are only a finite number of real eigenvalues. As  $\varepsilon$  approaches  $-1$  from above, the number of real eigenvalues decreases to one, and this eigenvalue becomes infinite at  $\varepsilon = -1$ . In this paper it is shown that these qualitative spectral behaviors are generic and that they are exhibited by the eigenvalues of the general class of Hamiltonians  $H^{(2n)} = p^{2n} + x^2(ix)^\varepsilon$  ( $\varepsilon$  real,  $n = 1, 2, 3, \dots$ ). The complex classical behaviors of these Hamiltonians are also examined.

PACS numbers: 11.30.Er, 03.65.Db, 11.10.Ef

## I. EIGENVALUE BEHAVIORS

The well-studied family of  $\mathcal{PT}$ -symmetric Hamiltonians [1–5]

$$H = p^2 + x^2(ix)^\varepsilon \quad (\varepsilon \text{ real}) \quad (1)$$

is a continuous complex deformation in the parameter  $\varepsilon$  of the conventional harmonic-oscillator Hamiltonian  $p^2 + x^2$ . At  $\varepsilon = 0$  the eigenvalues of  $H$  are the usual harmonic-oscillator eigenvalues  $E_n = 2n + 1$  ( $n = 0, 1, 2, \dots$ ), but as  $\varepsilon$  varies away from 0, the eigenvalues exhibit several characteristic qualitative behaviors: When  $\varepsilon$  is positive, the eigenvalues are all real, positive, and discrete, and the eigenvalues increase as  $\varepsilon$  increases. When  $\varepsilon$  is negative, most of the eigenvalues are complex. As  $\varepsilon$  decreases from 0 to  $-1$ , the eigenvalues sequentially become pairwise degenerate and enter the complex plane as complex-conjugate pairs. As  $\varepsilon$  continues to decrease, eventually only one real eigenvalue remains, and this eigenvalue becomes infinite at  $\varepsilon = -1$  [6]. This behavior is displayed in Fig. 1.

The parametric region  $\varepsilon \geq 0$  is called the *region of unbroken  $\mathcal{PT}$  symmetry* because all of the eigenfunctions of the Hamiltonian are simultaneously eigenstates of  $\mathcal{PT}$ ; the parametric region  $\varepsilon < 0$  is called the *region of broken  $\mathcal{PT}$  symmetry* because the eigenfunctions of the Hamiltonian are not all eigenstates of  $\mathcal{PT}$  [7]. A phase transition at  $\varepsilon = 0$  separates the regions of unbroken and broken symmetry. Parametric families of  $\mathcal{PT}$ -symmetric Hamiltonians typically exhibit a phase transition with entirely real eigenvalues on one side and complex eigenvalues on the other. The  $\mathcal{PT}$  phase transition has been observed repeatedly in laboratory experiments [8–22].

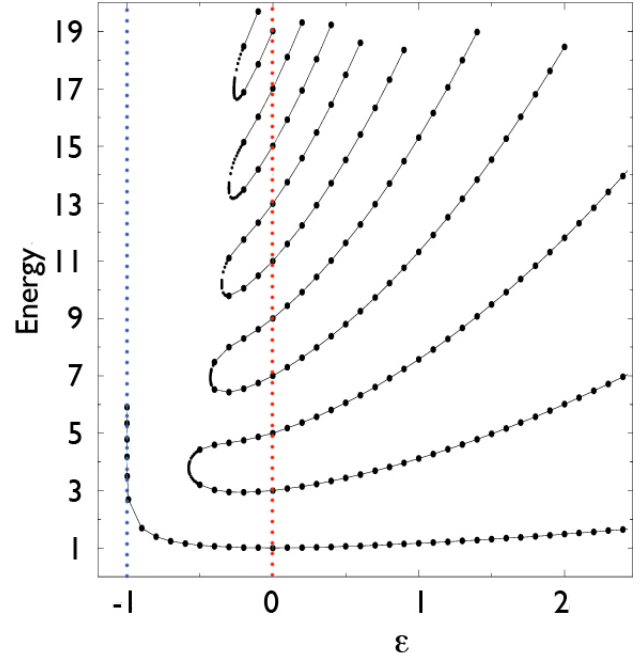


FIG. 1: Energy levels of the parametric family of Hamiltonians (1). When  $\varepsilon \geq 0$ , the eigenvalues are all real and positive, and increase with increasing  $\varepsilon$ . When  $\varepsilon$  decreases below 0, the eigenvalues disappear into the complex plane as complex conjugate pairs. Eventually, only one real eigenvalue remains when  $\varepsilon$  is less than about  $-0.57$ , and as  $\varepsilon$  approaches  $-1$  from above, this eigenvalue becomes infinite.

The purpose of this paper is to report our observation that the qualitative features of the eigenvalues of  $H$  in (1), as shown in Fig. 1, are generic; that is, the same qualitative behavior is displayed by the general family of Hamiltonians

$$H^{(2n)} = p^{2n} + x^2(ix)^\varepsilon \quad (\varepsilon \text{ real}; n = 1, 2, 3, \dots) \quad (2)$$

for which  $H$  in (1) is just  $H^{(2)}$ . For example, when  $n = 2$ , the time-independent eigenvalue problem  $H^{(4)}\psi = E\psi$  in coordinate space becomes the *fourth-order* differential

\*Current address: Department of Physics, King's College London, Strand, London, WC2R 2LS, UK

email: cmb@wustl.edu

†Current address: Theoretical Physics, Imperial College, London SW7 2AZ, UK

email: d.hook@imperial.ac.uk

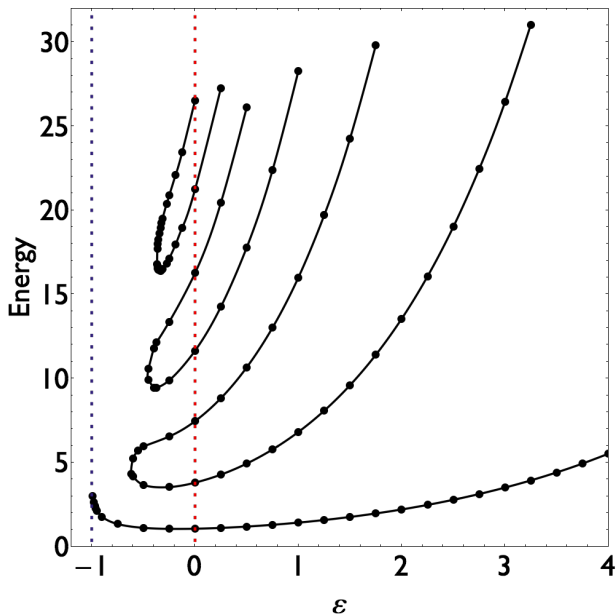


FIG. 2: Eigenvalues of the  $\mathcal{PT}$ -symmetric Hamiltonian  $H^{(4)}$  in (2) plotted as functions of  $\varepsilon$  for  $-1 < \varepsilon < 4$ . The eigenvalue behavior agrees qualitatively with that in Fig. 1 for the case of  $H^{(2)}$ .

equation

$$\frac{d^4}{dx^4}\psi(x) + x^2(ix)^\varepsilon\psi(x) = E\psi(x). \quad (3)$$

To determine the boundary conditions on  $\psi(x)$ , we begin with the requirement that  $\psi(x)$  vanish exponentially fast as  $|x| \rightarrow \infty$  on the real- $x$  axis when  $\varepsilon = 0$ , so the eigenvalues are the same as those of the conventionally Hermitian quartic-anharmonic-oscillator Hamiltonian  $p^2 + x^4$  [23]. Then, this eigenvalue problem is extended into the complex domain by allowing the parameter  $\varepsilon$  to range continuously from  $-1$  to  $+\infty$ . As we explain in Sec. II, this analysis determines the boundary conditions on  $\psi(x)$  in the complex- $x$  plane for real  $-1 < \varepsilon < \infty$ .

The eigenvalues of  $H^{(4)}$  are plotted in Fig. 2. The behaviors of the eigenvalues in Fig. 2 are qualitatively similar to the eigenvalues in Fig. 1. The eigenvalues in both cases are real, positive, and discrete for  $\varepsilon \geq 0$  and they become complex below the phase transition at  $\varepsilon = 0$ ; at  $\varepsilon = -1$  there are no eigenvalues at all.

When  $n = 3$ , the time-independent eigenvalue problem  $H^{(6)}\psi = E\psi$  is the *sixth-order* differential equation

$$-\frac{d^6}{dx^6}\psi(x) + x^2(ix)^\varepsilon\psi(x) = E\psi(x). \quad (4)$$

When  $\varepsilon = 0$ , the eigenvalues are the same as those of the conventionally Hermitian sextic-anharmonic-oscillator Hamiltonian  $p^2 + x^6$ . Observe that for  $-1 < \varepsilon < \infty$  the eigenvalues, which are shown in Fig. 3, behave qualitatively like those in Figs. 1 and 2.

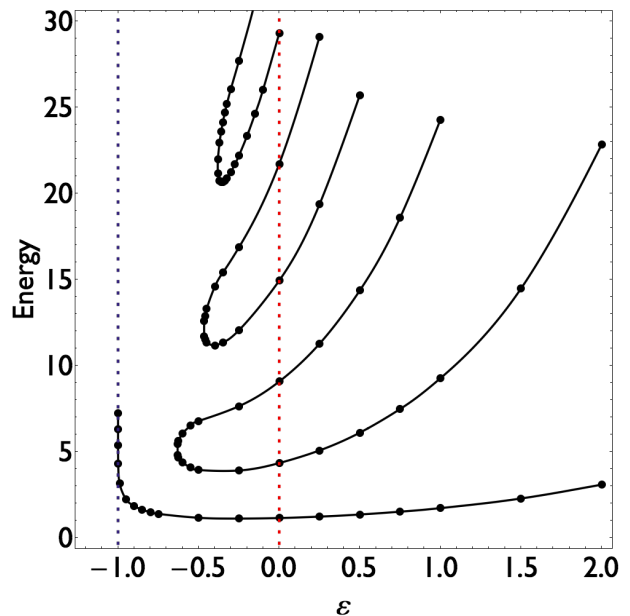


FIG. 3: Eigenvalues of the  $\mathcal{PT}$ -symmetric Hamiltonian  $H^{(6)}$  in (2) plotted as functions of  $\varepsilon$  for  $-1 < \varepsilon < 2$ . The eigenvalue behavior is qualitatively similar to that in Figs. 1 and 2 for  $H^{(2)}$  and  $H^{(4)}$ .

This paper is organized very simply: In Sec. II we explain the asymptotic and numerical analysis that leads to the results presented in Figs. 2 and 3. In Sec. III we study the complex classical trajectories associated with the Hamiltonians  $H^{(2)}$ ,  $H^{(4)}$ , and  $H^{(6)}$  for a variety of values of  $\varepsilon$ . These trajectories demonstrate some qualitative differences between these Hamiltonians. Finally, in Sec. IV we make some brief concluding remarks.

## II. ASYMPTOTIC AND NUMERICAL ANALYSIS

In this section we explain the techniques for calculating the eigenvalues that are graphed in Figs. 1–3. We begin by reviewing the procedure for finding the eigenvalues of  $H^{(2)}$ .

### A. Review of the case $H^{(2)}$

The properties of the eigenvalues of  $H^{(2)}$  were first elucidated in Ref. [1]. For completeness we give a brief review of the techniques that were used to construct an accurate plot of the eigenvalues.

The eigenvalue equation (the time-independent Schrödinger equation) for  $H^{(2)}$  reads

$$-\psi''(x) + x^2(ix)^\varepsilon\psi(x) = E\psi(x). \quad (5)$$

This differential equation has many different sets of eigenvalues, which are distinguished by the boundary condi-

tions imposed on the eigenfunctions. Thus, it is crucial to identify the specific boundary conditions on the eigenfunctions  $\psi(x)$  that give rise to the eigenvalues plotted in Fig. 1.

WKB theory can be used to obtain the possible asymptotic behaviors of  $\psi(x)$  for large  $|x|$ :

$$\psi(x) \sim \exp\left(\pm x^{2+\varepsilon/2} e^{i\pi\varepsilon/4}\right) \quad (|x| \rightarrow \infty), \quad (6)$$

where we have used  $i = e^{i\pi/2}$ . Since (5) is a second-order differential equation, there are two solutions; we want the solution that decays exponentially as  $|x| \rightarrow \infty$  on the real- $x$  axis when  $\varepsilon = 0$ .

To understand what happens when  $\varepsilon \neq 0$ , we let  $x = re^{i\theta}$  and require that as  $r \rightarrow \infty$ ,

$$\psi(r) \sim \exp\left\{-\frac{2}{4+\varepsilon} r^{2+\varepsilon/2} e^{i[\theta(2+\varepsilon/2)+\pi\varepsilon/4]}\right\}. \quad (7)$$

Note that  $\psi(r)$  vanishes in a Stokes wedge. At the center of the this wedge the phase, which is the expression in square brackets in (7), vanishes. This gives the angular location of the center of the wedge:

$$\theta_R = -\pi\varepsilon/(8+2\varepsilon). \quad (8)$$

We use the notation  $\theta_R$  here to indicate that this is the *right* Stokes wedge. There is also a *left* Stokes wedge, which is the mirror image of the right Stokes wedge; the angle of the center of the left Stokes wedge is called  $\theta_L$ . The mirror for this problem is the imaginary axis; the imaginary axis serves as the mirror because the Hamiltonian  $H^{(2)}$  is  $\mathcal{PT}$  symmetric. Note that  $\theta_R = 0$  at  $\varepsilon = 0$  and that  $\theta_R \rightarrow -\pi/2$  as  $\varepsilon \rightarrow \infty$ .

The opening angle  $\Delta\theta$  of the right Stokes wedge (and of the left Stokes wedge) is determined by requiring that the phase in square brackets in (7) is  $\pm\pi/2$ . This gives

$$\Delta\theta = 2\pi/(4+\varepsilon). \quad (9)$$

The opening angles of the Stokes wedges shrink to 0 as  $\varepsilon \rightarrow \infty$ . However, as  $\varepsilon \rightarrow -1$ , the opening angles expand to  $\Delta\theta/2 = \pi/3$ . Thus, since  $\theta_R = \pi/6$  at  $\varepsilon = -1$ , we see that the upper edge of the right wedge is at  $\theta_R + \Delta\theta/2 = \pi/2$ . At this value of  $\varepsilon$  the left and right wedges meet and the eigenvalue problem disappears because the integration contour can be deformed to infinity. This is an intuitive way to understand the rigorous result of Herbst that the spectrum becomes null when  $\varepsilon = -1$  [6].

The numerical calculation of the eigenvalues uses the standard *shooting method*. We integrate numerically with respect to the  $r$  variable down the centers of the left and right wedges and join the two solutions at the origin. The differential equation in the right wedge in the  $r$  variable reads

$$\psi_R''(r) = (r^{2+\varepsilon} + Ee^{2i\theta_R}) \psi_R(r) = Q(r)\psi_R(r). \quad (10)$$

The numerical integration begins at a large value of  $r$ , say  $r = r_0$ . To determine the appropriate initial conditions

at  $r = r_0$ , we use the WKB approximation for large  $r_0$ :

$$\psi_{\text{WKB}}(r_0) \sim KQ^{-1/4}(r_0) \exp\left[-\int_0^{r_0} dr \sqrt{Q(r)}\right], \quad (11)$$

where  $K$  is an arbitrary constant. We then adjust the constant  $K$  so that

$$\psi_R(r_0) = 1 \text{ and } \psi_R'(r_0) = -\sqrt{Q(r_0)}. \quad (12)$$

For the eigenvalues shown in Fig. 1 we choose  $r_0 = 12$ .

We patch the left and right solutions at the origin as follows: In the left wedge the eigenfunction that vanishes exponentially for large argument  $s$  is  $\alpha\psi_L(s)$ , and in the right wedge the eigenfunction that vanishes exponentially for large  $r$  is  $\beta\psi_R(r)$ , where  $\alpha$  and  $\beta$  are arbitrary constants. Thus, the patching conditions are

$$\alpha\psi_L(0) = \beta\psi_R(0), \quad \alpha e^{-i\theta_L}\psi_L'(0) = \beta e^{-i\theta_R}\psi_R'(0). \quad (13)$$

These are homogeneous linear equations, and thus by Cramer's rule the determinant  $D$  must vanish, where

$$D = \det\begin{pmatrix} \psi_R(0) & -\psi_L(0) \\ e^{-i\theta_R}\psi_R'(0) & -e^{-i\theta_L}\psi_L'(0) \end{pmatrix}. \quad (14)$$

The shooting procedure consists of adjusting the eigenvalue  $E$  so as to minimize  $|D|$ . This numerical procedure is highly efficient and gives a rapidly convergent sequence of numerical approximations to  $E$ .

## B. Case $H^{(4)}$

Let us consider the fourth-order differential-equation eigenvalue problem in (3). A local analysis of this differential equation for large  $|x|$  shows that, apart from multiplicative algebraic corrections, the four possible asymptotic behaviors of  $\psi(x)$  are

$$\psi(x) \sim \exp\left(\frac{4\omega}{6+\varepsilon} x^{(6+\varepsilon)/4} e^{i\pi\varepsilon/8}\right) \quad (|x| \rightarrow \infty), \quad (15)$$

where  $\omega^4 = -1$ . We must exclude two of these four solutions because they grow exponentially when  $|x| \gg 1$ .

We now describe the Stokes wedges that are associated with the solutions. We let  $x = re^{i\theta}$ , and in the right Stokes wedge we set  $\theta = \theta_R$ . Neglecting for the moment the effect of  $\omega$ , the phase angle in (15) is  $(6+\varepsilon)\theta_R/4 + \pi\varepsilon/8$ . This angle vanishes at the center of the Stokes wedge. Thus,

$$\theta_R = -\pi\varepsilon/(12+2\varepsilon). \quad (16)$$

As in the case of  $H^{(2)}$ , the center of the wedge is located at  $\theta_R = 0$  when  $\varepsilon = 0$ , and the center rotates downward (clockwise) to  $-\pi/2$  as  $\varepsilon \rightarrow \infty$ .

As before, the opening angle  $\Delta\theta$  of the Stokes wedge is determined by the condition that the phase has the value  $\pm\pi/2$ . This gives

$$\Delta\theta = 4\pi/(6+\varepsilon). \quad (17)$$

Thus, the opening angle is  $2\pi/3$  at  $\varepsilon = 0$  and the opening angle vanishes as  $\varepsilon \rightarrow \infty$ .

We now observe one of the universal features of the Hamiltonians in (2). At  $\varepsilon = -1$ ,  $\theta_R = \pi/10$  and  $\Delta\theta/2 = 4\pi/10$ . Thus, the upper edge of the right wedge is at  $\theta_R + \Delta\theta/2 = \pi/2$ . By  $\mathcal{PT}$  symmetry, there is a left wedge (a mirror reflection of the right wedge) in the left-half plane. The center of the left wedge is at the angle  $\theta_L = -\pi + \theta_R$ . Hence, when  $\varepsilon = -1$ , the left and the right wedges touch, the eigenvalue problem collapses, and the spectrum becomes null. (This is the generalization of the effect that Herbst found for the Hamiltonian  $H = p^2 \pm ix$  [6].) This collapse of the eigenvalue problem is a universal phenomenon and always occurs at  $\varepsilon = -1$  for all Hamiltonians in (2).

We now explain the numerical procedure for finding the eigenvalues in Fig. 2. In the right wedge we substitute  $x = re^{i\theta_R}$  in the differential equation (3) and obtain

$$\psi_R^{(4)}(r) = -(r^{2+\varepsilon} + Ee^{4i\theta_R})\psi_R(r) = -Q(r)\psi_R(r). \quad (18)$$

There are two solutions that grow exponentially with  $r$  and two solutions that vanish exponentially with  $r$ .

Until now,  $\omega$  has not played any part in the analysis. However, it plays a crucial role in determining the boundary conditions. We integrate numerically downward in  $r$

from a large value of  $r = r_0$ . To fix the initial conditions we use the WKB approximation for fourth-order differential equations [24]:

$$\psi_{\text{WKB}}(r_0) \sim KQ^{-\frac{3}{8}}(r_0) \exp\left[\omega \int_0^{r_0} dr Q^{1/4}(r)\right], \quad (19)$$

where  $\omega^4 = -1$ . We choose the constant  $K$  so that

$$\psi_R(r_0) = 1. \quad (20)$$

Then, using  $\omega_1 = e^{3\pi i/4}$  and  $\omega_2 = e^{-3\pi i/4}$  so that the solution decays exponentially, we take

$$\psi_{R,j}^{(k)}(r_0) = \omega_j^k Q^{(k/4)}(r_0), \quad (21)$$

where  $\psi_{R,j}^{(k)}$  is the  $k$ th derivative with respect to  $r$ . We then choose a large number for  $r_0$ , say  $r_0 = 12$ . The solution in the left wedge is

$$\psi_L = \alpha_1\psi_{L,1} + \alpha_2\psi_{L,2} \quad (22)$$

and the solution in the right wedge is

$$\psi_R = \beta_1\psi_{R,1} + \beta_2\psi_{R,2}. \quad (23)$$

We must now patch the left and right solutions at  $r = 0$ . To do so we require that the eigenfunctions  $\psi_L$  and  $\psi_R$  be continuous and have continuous first, second, and third derivatives at  $r = 0$ . These four conditions are written as a system of four linear equations for  $\alpha_1$ ,  $\alpha_2$ ,  $\beta_1$ , and  $\beta_2$ :

$$\begin{aligned} \alpha_1\psi_{L,1}(0) + \alpha_2\psi_{L,2}(0) &= \beta_1\psi_{R,1}(0) + \beta_2\psi_{R,2}(0), \\ \alpha_1e^{-i\theta_L}\psi'_{L,1}(0) + \alpha_2e^{-i\theta_L}\psi'_{L,2}(0) &= \beta_1e^{-i\theta_R}\psi'_{R,1}(0) + \beta_2e^{-i\theta_R}\psi'_{R,2}(0), \\ \alpha_1e^{-2i\theta_L}\psi''_{L,1}(0) + \alpha_2e^{-2i\theta_L}\psi''_{L,2}(0) &= \beta_1e^{-2i\theta_R}\psi''_{R,1}(0) + \beta_2e^{-2i\theta_R}\psi''_{R,2}(0), \\ \alpha_1e^{-3i\theta_L}\psi'''_{L,1}(0) + \alpha_2e^{-3i\theta_L}\psi'''_{L,2}(0) &= \beta_1e^{-3i\theta_R}\psi'''_{R,1}(0) + \beta_2e^{-3i\theta_R}\psi'''_{R,2}(0). \end{aligned} \quad (24)$$

Because these patching conditions are homogeneous equations, they translate via Cramer's rule to the condition that the following  $4 \times 4$  determinant of the coefficients vanishes:

$$D = \det \begin{pmatrix} \psi_{R,1}(0) & \psi_{R,2}(0) & -\psi_{L,1}(0) & -\psi_{L,2}(0) \\ e^{-i\theta_R}\psi'_{R,1}(0) & e^{-i\theta_R}\psi'_{R,2}(0) & -e^{-i\theta_L}\psi'_{L,1}(0) & -e^{-i\theta_L}\psi'_{L,2}(0) \\ e^{-2i\theta_R}\psi''_{R,1}(0) & e^{-2i\theta_R}\psi''_{R,2}(0) & -e^{-2i\theta_L}\psi''_{L,1}(0) & -e^{-2i\theta_L}\psi''_{L,2}(0) \\ e^{-3i\theta_R}\psi'''_{R,1}(0) & e^{-3i\theta_R}\psi'''_{R,2}(0) & -e^{-3i\theta_L}\psi'''_{L,1}(0) & -e^{-3i\theta_L}\psi'''_{L,2}(0) \end{pmatrix}. \quad (25)$$

The objective of the numerical shooting procedure is to find the values of  $E$  that minimize this determinant.

### C. Case $H^{(6)}$

For the eigenvalue problem in (4) the possible asymptotic behaviors for large  $|x|$  (excluding algebraic correc-

tions) are given by

$$\psi(x) \sim \exp\left(\frac{6\omega}{8+\varepsilon}x^{(8+\varepsilon)/6}e^{i\pi\varepsilon/12}\right) \quad (|x| \rightarrow \infty), \quad (26)$$

where  $\omega^6 = 1$ .

There are six solutions, but we seek the three solutions that vanish as  $|x| \rightarrow \infty$ . We substitute  $x = re^{i\theta_R}$  in (26), and we require that the solution vanish as  $r \rightarrow \infty$ . Apart from  $\omega$ , the phase angle in the asymptotic behavior

vanishes when

$$\theta_R = -\pi\varepsilon/(16 + 2\varepsilon). \quad (27)$$

This determines the center of the right wedge. At  $\varepsilon = 0$ ,  $\theta_R = 0$  and as  $\varepsilon \rightarrow \infty$ ,  $\theta_R \rightarrow -\pi/2$ , just as before.

The opening angle  $\Delta\theta$  of the wedge is determined by requiring that the phase have the value  $\pm\pi/2$ . This gives

$$\Delta\theta = 6\pi/(8 + \varepsilon). \quad (28)$$

At  $\varepsilon = 0$  the opening angle is  $3\pi/4$  and this angle vanishes as  $\varepsilon \rightarrow \infty$ .

From (27) and (28) we see that at  $\varepsilon = -1$ ,  $\theta_R = \pi/14$  and  $\Delta\theta/2 = 6\pi/14$ . Thus, the upper edge of the wedge is at  $\theta_R + \Delta\theta/2 = \pi/2$ . At this value of  $\varepsilon$ , the left and right wedges touch and the eigenvalue problem disappears, just as in the case of  $H^{(2)}$  and  $H^{(4)}$ .

To find the eigenvalues using the numerical shooting method, we integrate down the center of the left and right wedges and patch the solutions at the origin. In the right wedge the differential equation in the  $r$  variable is

$$\psi_R^{(6)}(r) = (r^{2+\varepsilon} + Ee^{6i\theta_R}) \psi_R(r) = Q(r)\psi_R(r). \quad (29)$$

In each wedge there are three exponentially decaying solutions and three exponentially growing solutions. We

select the decaying solutions by applying the appropriate boundary conditions at a large value of  $r = r_0 = 12$ . To identify the appropriate initial conditions for the numerical integration, we use the WKB approximation for large  $r_0$ :

$$\psi_{\text{WKB}}(r_0) \sim KQ^{-\frac{5}{12}}(r_0) \exp\left[\omega \int_0^{r_0} dr Q^{1/6}(r)\right], \quad (30)$$

where  $\omega_1 = -1$ ,  $\omega_2 = e^{2\pi i/3}$ , and  $\omega_3 = e^{-2\pi i/3}$ . We adjust the constant  $K$  such that

$$\psi_R(r_0) = 1. \quad (31)$$

Then,

$$\psi_{R,j}^{(k)}(r_0) = \omega_j^k Q^{(k/6)}(r_0). \quad (32)$$

The solution in the left wedge is

$$\psi_L = \alpha_1\psi_{L,1} + \alpha_2\psi_{L,2} + \alpha_3\psi_{L,3} \quad (33)$$

and the solution in the right wedge is

$$\psi_R = \beta_1\psi_{R,1} + \beta_2\psi_{R,2} + \beta_3\psi_{R,3}. \quad (34)$$

The patching conditions give a vanishing determinant via Cramer's rule, where the determinant is

---


$$D = \det \begin{pmatrix} \psi_{R,1}(0) & \psi_{R,2}(0) & \psi_{R,3}(0) & -\psi_{L,1}(0) & -\psi_{L,2}(0) & -\psi_{L,3}(0) \\ e^{-i\theta_R}\psi'_{R,1}(0) & e^{-i\theta_R}\psi'_{R,2}(0) & e^{-i\theta_R}\psi'_{R,3}(0) & -e^{-i\theta_L}\psi'_{L,1}(0) & -e^{-i\theta_L}\psi'_{L,2}(0) & -e^{-i\theta_L}\psi'_{L,3}(0) \\ e^{-2i\theta_R}\psi''_{R,1}(0) & e^{-2i\theta_R}\psi''_{R,2}(0) & e^{-2i\theta_R}\psi''_{R,3}(0) & -e^{-2i\theta_L}\psi''_{L,1}(0) & -e^{-2i\theta_L}\psi''_{L,2}(0) & -e^{-2i\theta_L}\psi''_{L,3}(0) \\ e^{-3i\theta_R}\psi'''_{R,1}(0) & e^{-3i\theta_R}\psi'''_{R,2}(0) & e^{-3i\theta_R}\psi'''_{R,3}(0) & -e^{-3i\theta_L}\psi'''_{L,1}(0) & -e^{-3i\theta_L}\psi'''_{L,2}(0) & -e^{-3i\theta_L}\psi'''_{L,3}(0) \\ e^{-4i\theta_R}\psi^{(4)}_{R,1}(0) & e^{-4i\theta_R}\psi^{(4)}_{R,2}(0) & e^{-4i\theta_R}\psi^{(4)}_{R,3}(0) & -e^{-4i\theta_L}\psi^{(4)}_{L,1}(0) & -e^{-4i\theta_L}\psi^{(4)}_{L,2}(0) & -e^{-4i\theta_L}\psi^{(4)}_{L,3}(0) \\ e^{-5i\theta_R}\psi^{(5)}_{R,1}(0) & e^{-5i\theta_R}\psi^{(5)}_{R,2}(0) & e^{-5i\theta_R}\psi^{(5)}_{R,3}(0) & -e^{-5i\theta_L}\psi^{(5)}_{L,1}(0) & -e^{-5i\theta_L}\psi^{(5)}_{L,2}(0) & -e^{-5i\theta_L}\psi^{(5)}_{L,3}(0) \end{pmatrix}. \quad (35)$$


---

We shoot so as to minimize this determinant.

### III. CLASSICAL TRAJECTORIES

While the eigenvalues of the quantum-mechanical Hamiltonians  $H^{(2n)}$  are qualitatively similar, the classical-mechanical trajectories for these Hamiltonians exhibit marked differences. Using the numerical techniques described in Ref. [2], we have studied the complex classical trajectories associated with the Hamiltonians in (2) for  $\varepsilon = 0, 2, 4$ , and  $6$ . In Fig. 4 we plot four trajectories in  $x$  space and in  $p$  space for  $n = 1$  for these values of  $\varepsilon$  and in Fig. 5 we show corresponding plots for  $n = 2$ . Figures 6 and 7 display the corresponding plots for  $n = 3$ , and in these figures we can see the emergence of new kinds of topological structures. Figures 4-7 show

a progressively increasing topological complexity, which arises because of the higher powers of  $p$  in the Hamiltonians. It is interesting that the pattern of the eigenvalues in Figs. 1-3 shows no corresponding qualitative changes.

### IV. CONCLUDING REMARKS

We have shown that the key qualitative features of the eigenvalue problem associated with  $H^{(2n)}$  in (2) are universal. In particular, (i) the critical point between the regions of broken and unbroken symmetry is always at  $\varepsilon = 0$ , (ii) the lower end of the broken region is always at  $\varepsilon = -1$  at which point the spectrum becomes null, and (iii) the eigenvalues are positive and rise with increasing  $\varepsilon$  in the unbroken region.

Qualitative differences between these Hamiltonians are

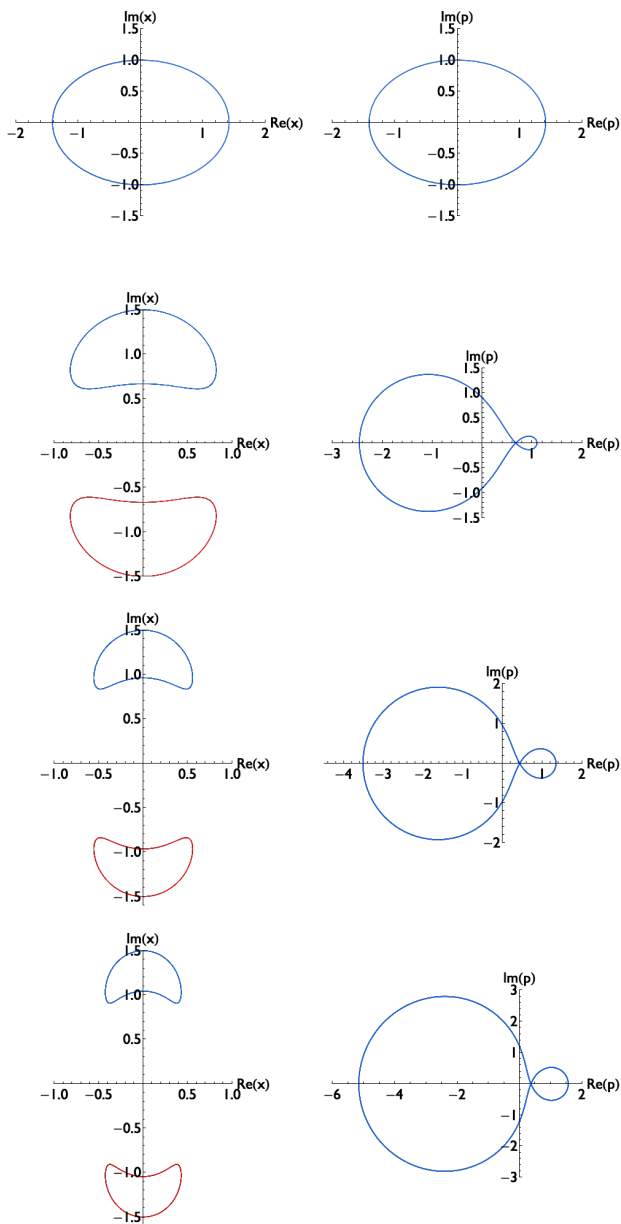


FIG. 4: Complex classical trajectories of the Hamiltonians  $H^{(2)} = p^2 + x^2(ix)^\varepsilon$ , where  $\varepsilon = 0$  (first row),  $\varepsilon = 2$  (second row),  $\varepsilon = 4$  (third row), and  $\varepsilon = 6$  (fourth row). The left column is the projection of the classical trajectory in the complex- $x$  plane and the right column is the projection of the trajectory in the complex- $p$  plane. In every case the classical energy is 1. For the cases  $\varepsilon = 2, 4$ , and  $6$  *two* trajectories are shown in the left column (blue and red online). The corresponding complex- $p$ -plane trajectories do not cross, but rather lie on a two-sheeted Riemann surface. The  $p$ -plane trajectories appear to be coincident because they are projected onto a single complex plane.

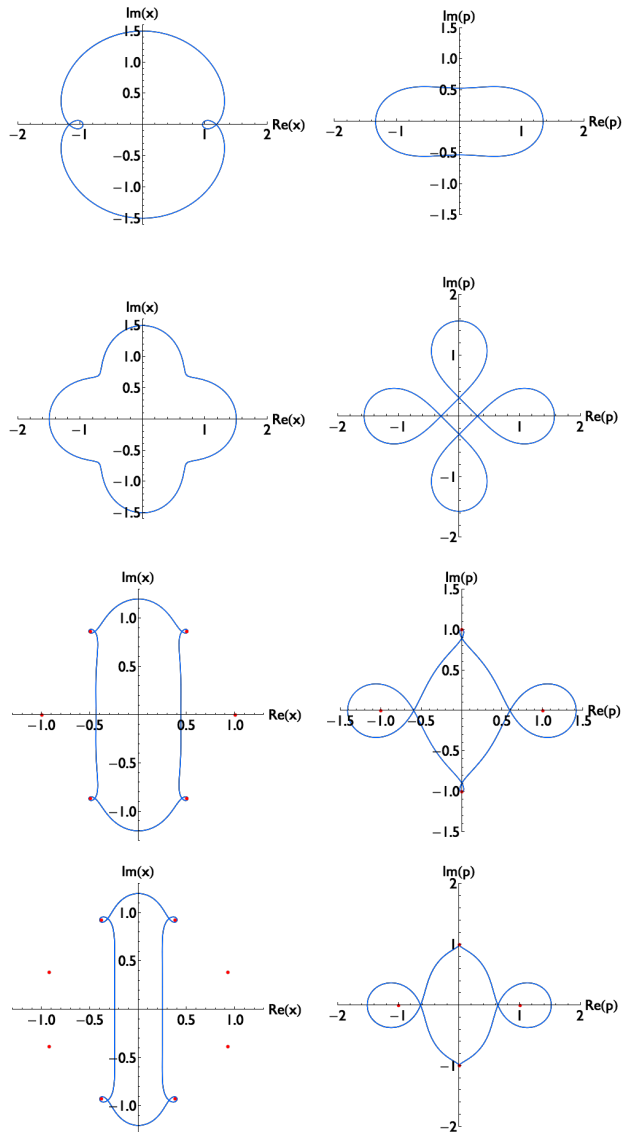


FIG. 5: Same as Fig. 4 panel except that  $n = 2$ . However, in this case we do not observe up-down trajectory pairing in the complex- $x$  plane.

much easier to spot at the classical level. We see that as  $n$  increases, the classical trajectories develop new and richer topologies. Near the turning points the trajectories share the same features as those studied in Ref. [25], in which the classical paths for higher-derivative Hamiltonians were also investigated.

CMB thanks the Leverhulme Foundation and the U.S. Department of Energy for financial support. Mathematica was used to perform numerical calculations.

[1] C. M. Bender and S. Boettcher, *Phys. Rev. Lett.* **80**, 5243 (1998).

[2] C. M. Bender, S. Boettcher, and P. N. Meisinger,

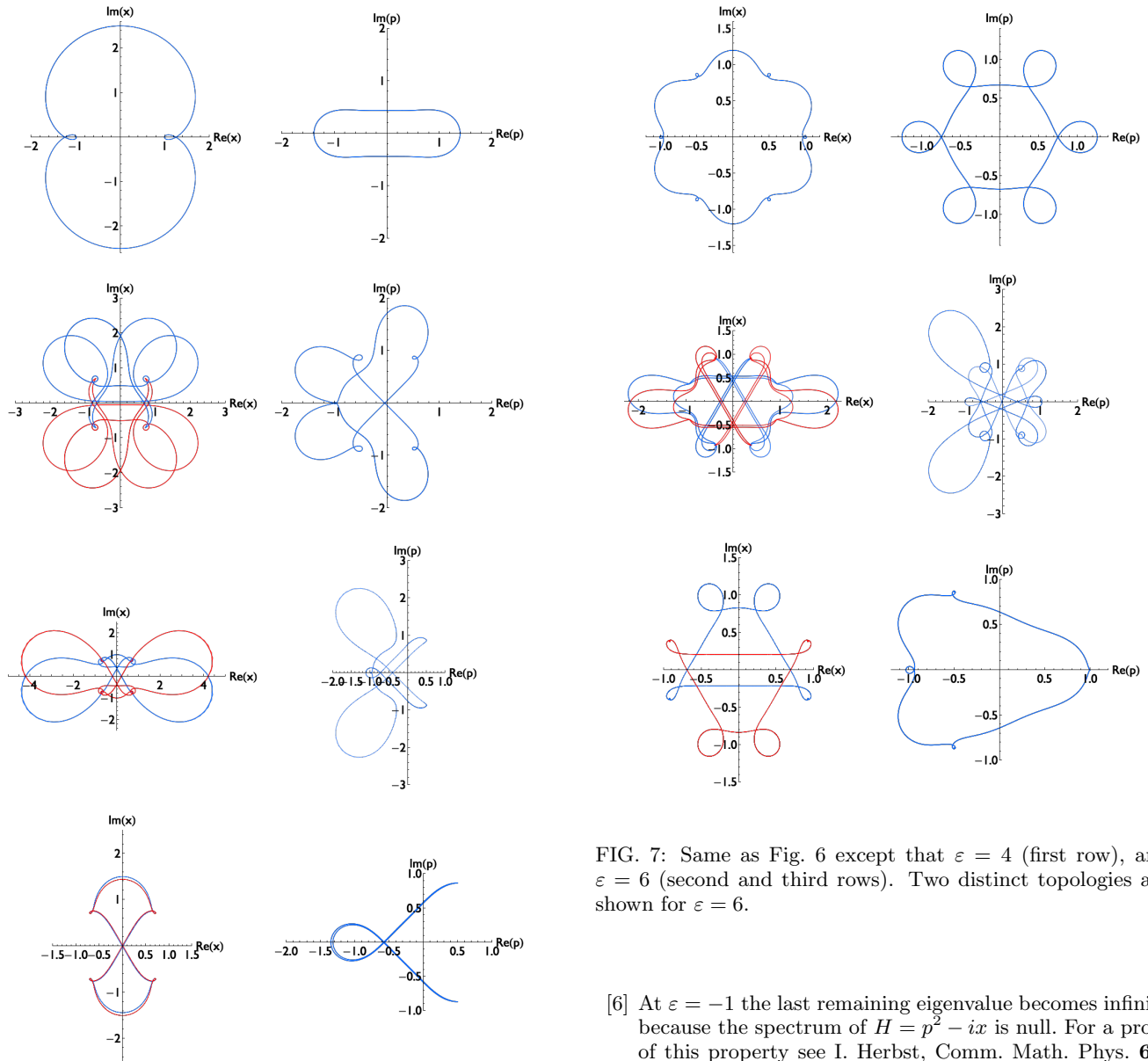


FIG. 6: Complex classical trajectories of the Hamiltonians  $H^{(6)} = p^6 + x^2(ix)^\varepsilon$ , where  $\varepsilon = 0$  (first row),  $\varepsilon = 2$  (second, third, and fourth rows). The left column is the projection of the classical trajectory in the complex- $x$  plane and the right column is the projection of the trajectory in the complex- $p$  plane. In every case the classical energy is 1. In rows 2, 3, and 4 three distinct topologies are shown. As in Fig. 4, these trajectories come in up-down symmetric pairs (blue and red online). The corresponding complex- $p$ -plane trajectories do not cross, but rather lie on a six-sheeted Riemann surface.

*J. Math. Phys.* **40**, 2201 (1999).

[3] C. M. Bender, *Rep. Prog. Phys.* **70**, 947 (2007).

[4] P. E. Dorey, C. Dunning, and R. Tateo, *J. Phys. A: Math. Gen.* **34**, L391 (2001) and **34**, 5679 (2001).

[5] P. E. Dorey, C. Dunning, and R. Tateo, *J. Phys. A: Math. Gen.* **40**, R205 (2007).

FIG. 7: Same as Fig. 6 except that  $\varepsilon = 4$  (first row), and  $\varepsilon = 6$  (second and third rows). Two distinct topologies are shown for  $\varepsilon = 6$ .

- [6] At  $\varepsilon = -1$  the last remaining eigenvalue becomes infinite because the spectrum of  $H = p^2 - ix$  is null. For a proof of this property see I. Herbst, *Comm. Math. Phys.* **64**, 279 (1979).
- [7] C. M. Bender, D. C. Brody, and H. F. Jones, *Phys. Rev. Lett.* **89**, 270401 (2002).
- [8] J. Rubinstein, P. Sternberg, and Q. Ma, *Phys. Rev. Lett.* **99**, 167003 (2007).
- [9] A. Guo, G. J. Salamo, D. Duchesne, R. Morandotti, M. Volatier-Ravat, V. Aimez, G. A. Siviloglou, and D. N. Christodoulides, *Phys. Rev. Lett.* **103**, 093902 (2009).
- [10] C. E. Rüter, K. G. Makris, R. El-Ganainy, D. N. Christodoulides, M. Segev, and D. Kip, *Nat. Phys.* **6**, 192 (2010).
- [11] K. F. Zhao, M. Schaden, and Z. Wu, *Phys. Rev. A* **81**, 042903 (2010).
- [12] Y. D. Chong, L. Ge, and A. D. Stone, *Phys. Rev. Lett.* **106**, 093902 (2011).
- [13] Z. Lin, H. Ramezani, T. Eichelkraut, T. Kottos, H. Cao, and D. N. Christodoulides, *Phys. Rev. Lett.* **106**, 213901 (2011).
- [14] C. Zheng, L. Hao, and G. L. Long, arXiv:1105.6157 [quant-ph] (2011).

- [15] J. Schindler, A. Li, M. C. Zheng, F. M. Ellis, T. Kottos, *Phys. Rev. A* **84**, 040101 (2011).
- [16] L. Feng, M. Ayache, J. Huang, Y.-L. Xu, M.-H. Lu, Y.-F. Chen, Y. Fainman, and A. Scherer, *Science* **333**, 729 (2011).
- [17] M. Fagotti, C. Bonati, D. Logoteta, P. Marconcini, and M. Macucci, *Phys. Rev. B* **83**, 241406(R) (2011).
- [18] Z. Lin, J. Schindler, F. M. Ellis, and T. Kottos, *Phys. Rev. A* **85**, 050101 (2012).
- [19] S. Bittner, B. Dietz, U. Guenther, H. L. Harney, M. Miski-Oglu, A. Richter, and F. Schaefer, *Phys. Rev. Lett.* **108**, 024101 (2012).
- [20] A. Szameit, M. C. Rechtsman, O. Bahat-Treidel, and M. Segev, *Phys. Rev. A* **84**, 021806(R) (2011).
- [21] M. Liertzer, L. Ge, A. Cerjan, A. D. Stone, H. E. Tureci, and S. Rotter, *Phys. Rev. Lett.* **108**, 173901 (2012).
- [22] A. Zezyulin and V. V. Konotop, *Phys. Rev. Lett.* (accepted April 16, 2012)
- [23] For the numerical values of these eigenvalues, see C. M. Bender and S. A. Orszag, *Advanced Mathematical Methods for Scientists and Engineers* (McGraw Hill, New York, 1978), Table 10.4.
- [24] See Ref. [23], Chap. 10.
- [25] C. M. Bender and D. W. Hook, *J. Phys. A: Math. Theor.* **41**, 244005 (2008).